

Swift, NuStar and XMM-Newton observations of the NLS1 galaxy RX J2317.8–4422 in an extreme X-ray low flux state

Dirk Grupe^{1*}, S. Komossa², Luigi Gallo³, Norbert Schartel⁴, Michael Parker^{4,5}, Maria Santos-Lleo⁴, Andrew C. Fabian⁵, Fiona Harrison⁶, Giovanni Miniutti⁷

¹Department of Earth and Space Sciences, Morehead State University, Morehead, KY 40514, USA

²Max-Planck-Institut für Radioastronomie, Auf dem Hügel 69, 53111 Bonn, Germany

³Saint Mary's University, Department of Astronomy & Physics, 923 Robie Street, Halifax, Canada, B3H 3C3

⁴European Space Astronomy Centre (ESAC), P.O. Box, 78, E-28691 Villanueva de la Cañada, Madrid, Spain

⁵Institute of Astronomy, University of Cambridge, Madingley Road, CB3 0HA Cambridge, UK

⁶Cahill Center for Astrophysics, California Institute of Technology, 1216 East California Boulevard, Pasadena, CA 91125, USA

⁷Departamento de Astrofísica, Centro de Astrobiología (CSIC-INTA), Campus ESA-ESAC, Villanueva de la Cañada, 28692 Madrid, Spain

Accepted XXX. Received YYY; in original form ZZZ

ABSTRACT

We report the discovery of RX J2317.8–4422 in an extremely low X-ray flux state by the *Neil Gehrels Swift* observatory in 2014 April/May. In total, the low-energy X-ray emission dropped by a factor 100. We have carried out multi-wavelength follow-up observations of this Narrow-Line Seyfert 1 galaxy. Here we present observations with *Swift*, *XMM-Newton*, and *NuSTAR* in October and November 2014 and further monitoring observations by *Swift* from 2015 to 2018. Compared with the beginning of the *Swift* observations in 2005, in the November 2014 *XMM-Newton* and *NuSTAR* observation RX J2317–4422.8 dropped by a factor of about 80 in the 0.3–10 keV band. While the high-state *Swift* observations can be interpreted by a partial covering absorption model with a moderate absorption column density of $N_H = 5.4 \times 10^{22}$ cm⁻² or blurred reflection, due to dominating background at energies above 2 keV the low-state *XMM-Newton* data can not distinguish between different multi-component models and were adequately fit with a single power-law model. We discuss various scenarios like a long-term change of the accretion rate or absorption as the cause for the strong variability seen in RX J2317.8–4422.

Key words: galaxies: Seyfert - quasars: individual: RX J2317.8–4422 - galaxies: nuclei

1 INTRODUCTION

Extremes of AGN variability provide us with a powerful tool of understanding the physics of the central engine of Active Galactic Nuclei (AGN). While AGN typically vary on all time scales by factors of a few, some of these exhibit dramatic drops in their X-ray fluxes by factors that can exceed 100. The cause of these transitions into deep minimum X-ray flux states in AGN can be associated with (a) dramatic changes in the accretion rate onto the central supermassive black hole (SMBH), (b) changes in absorption, or (c) changes in (relativistically blurred) reflection of coronal X-ray photons off the accretion disc, for instance in response to changes in the lamppost height or luminosity. All three of these types of events have been identified in the past. A good example of an AGN

that has exhibited a dramatic change in its accretion rate is the Seyfert 1.9 galaxy IC 3599 (Grupe et al. 1995a; Brandt et al. 1995; Komossa & Bade 1999; Grupe et al. 2015). X-ray reflection has been suggested to be the cause of the strong X-ray flux changes in AGN which we have examined in the past based on *XMM-Newton* observations of AGN such as Mkn 335 (Grupe et al. 2008a, 2012; Gallo et al. 2013; Komossa et al. 2014; Gallo et al. 2015, 2018; Wilkins et al. 2015) and 1H0707–495 (Fabian et al. 2012). The third explanation of huge flux changes in AGN is absorption, in particular partial-covering absorption in X-rays (e.g. Komossa & Fink 1997; Guainazzi et al. 1998; Gallagher et al. 2004; Risaliti et al. 2005; Bianchi et al. 2009; Mizumoto et al. 2014; Parker et al. 2014; Yamasaki et al. 2016; Zhang et al. 2017; Turner et al. 2018).

Perhaps the best example of an extreme X-ray absorption event is the Narrow Line Seyfert 1 galaxy (NLS1)

* E-mail: d.grupe@moreheadstate.edu

WPVS 007 (Grupe et al. 1995; Grupe et al. 2013). While the cause of the dramatic X-ray drop in this NLS1 had been a mystery for a decade, it became clear from FUSE observations, that this low-luminosity, low black hole mass AGN shows extremely strong broad absorption line troughs in the UV (Leighly et al. 2009). Observations by *Swift*, HST, and *Chandra* suggest that we most likely see the AGN through and above a patchy, dusty torus (Leighly et al. 2015).

We have an ongoing fill-in program with the *Neil Gehrels Gamma-Ray Burst Explorer Mission Swift* (*Swift* throughout the paper, Gehrels et al. 2004) to check on the X-ray flux of a sample of AGN (Grupe et al. 2010). In addition, AGN that go through extreme flux changes have been discovered through the *XMM-Newton* Slew Survey (Saxton et al. 2008). These programs have led to the discovery of several AGN that undergo transitions into deep minimum X-ray flux states or display dramatic flux increases allowing us to trigger *XMM-Newton* and *NuSTAR* observations.

Besides Mkn 335 and 1H0707–495, we also successfully observed Mkn 1048, PG 0844+349, PG 0043+039, PG 2112+059, PG 1535+547, and HE 1136–2304 (Parker et al. 2014; Gallo et al. 2011; Kollatschny et al. 2015, 2016; Schartel et al. 2007, 2010; Ballo et al. 2008; Parker et al. 2016; Komossa et al. 2017; Zetzl et al. 2018) with *XMM-Newton* and *NuSTAR*. One of the most recent AGN discovered as part of this survey was RX J2317.8–4422 ($\alpha_{2000} = 23^{\text{h}} 17^{\text{m}} 50^{\text{s}}$, $\delta_{2000} = -44^{\circ} 22' 27''$, $z=0.134$). RX J2317–4422 was first detected as a bright X-ray AGN during the ROSAT All-Sky Survey (RASS, Voges et al. 1999; Schwobe et al. 2000) and was found to be an AGN with a very steep X-ray spectrum with $\alpha_x = 2.5 \pm 0.8$ (Grupe et al. 1998). From its optical spectrum it was identified to be a NLS1 (Grupe et al. 1999) with a black hole mass of $M_{\text{BH}} = 7.5 \times 10^6 M_{\odot}$ (see Sect. 3.4) accreting near the Eddington limit. A follow-up observation with ROSAT in 1997 May did not suggest any dramatic changes in its X-ray flux (Grupe et al. 2001).

Swift started observing RX J2317–4422 in 2005 May as a calibration target (Grupe et al. 2010). *Swift* continued to observe RX J2317–4422 several times as part of various fill-in programs. While none of these observations suggested anything special about this NLS1, an observation in April 2014 revealed that it had dropped its X-ray flux dramatically by a factor of more than 30 compared to the previous *Swift* observations within less than a year. After the discovery of this very low X-ray flux, we performed additional *Swift* observations, confirming the low flux state. This confirmation allowed us to trigger a 20 ks initial *XMM-Newton* observation in 2014 October to obtain a preliminary low state spectrum, which then led to an additional 100ks ToO observation with *XMM-Newton* in conjunction with *NuSTAR* in 2014 November. These *XMM-Newton* and *NuSTAR* observations are the main focus of our paper.

The outline of this paper is as follows: in § 2 we describe the data reduction of the *Swift*, *XMM-Newton* and *NuSTAR* observations. In § 3 we present the results from the analysis of the light curves and X-ray spectroscopy, and in § 4 we provide a discussion of the nature of the X-ray low-state of RX J2317–4422. Throughout the paper spectral indices are denoted as energy spectral indices with $F_{\nu} \propto \nu^{-\alpha}$. Luminosities are calculated assuming a Λ CDM cosmology with $\Omega_{\text{M}}=0.286$, $\Omega_{\Lambda}=0.714$ and a Hubble constant of $H_0=70$ km

$\text{s}^{-1} \text{Mpc}^{-1}$. This results in a luminosity distance $D=631$ Mpc using the cosmology calculator by Wright (2006). All uncertainties are 1σ unless stated otherwise. The Galactic foreground absorption in the direction of RX J2317–4422 has a column density of $N_{\text{H}} = 1.07 \times 10^{20} \text{ cm}^{-2}$ (Kalberla et al. 2005). For all statistical analysis we use the R package, version 3.2.4 (e.g., Crawley 2009).

2 OBSERVATIONS AND DATA REDUCTION

2.1 Swift

Table 1 lists the *Swift* observations of RX J2317–4422 starting with the first observation in May 2005. The *Swift* X-ray telescope (XRT; Burrows et al. 2005) was operating in photon counting mode (Hill et al. 2004). Source counts were selected in a circle with a radius of $23.6''$ and background counts in a nearby circular region with a radius of $235.7''$. The 3σ upper limits and the count rates of the detections were determined by applying the Bayesian method by Kraft et al. (1991). Some of the detections allowed a spectral analysis using Cash statistics (Cash 1979). For all spectra we used the most recent response file *swxpc0to12s6_20130101v014.rmf*. The X-ray spectra were analyzed using *XSPEC* version 12.9.1p (Arnaud 1996).

In case spectra could not be extracted from the data we converted the count rates or upper limits with an energy conversion factor of $3.61 \times 10^{-14} \text{ W m}^{-2} (\text{counts s}^{-1})^{-1}$ which was derived from the early observations when RX J2317–4422 was in a high state. Note that the spectrum most likely changed. However, due to the low count rate of RX J2317–4422 no spectral information could be derived from the *Swift* XRT data during the low state since 2014.

The UV-optical telescope (UVOT; Roming et al. 2005) data of each segment were coadded in each filter with the UVOT task *wotimsum*. Source counts in all 6 UVOT filters were selected in a circle with a radius of $7''$ and background counts in a nearby source free region with a radius of $20''$. The background corrected counts were converted into magnitudes and fluxes by using the calibration as described in Poole et al. (2008) and Breeveld et al. (2010). UVOT Vega magnitudes and fluxes were measured with the task *wot-source*. The UVOT data were corrected for Galactic reddening ($E_{\text{B}-\text{V}} = 0.012$; Schlegel et al. 1998). The correction factor in each filter was calculated according to equation (2) in Roming et al. (2009) who used the standard reddening correction curves by Cardelli et al. (1989).

Note that the $7''$ source extraction radius, which is larger than the standard $5''$ radius, was necessary because during several observations the *Swift* star tracker was unable to lock onto the target and *Swift* started to drift causing the image to be smeared out. This drift has two major effects: 1) enhanced background in the source extraction region, and 2) possible host galaxy contamination of the central source. However, at the redshift of RX J2317–4422 we do not expect the contribution of widely extended host emission at these radii. A point-like host contribution cannot be excluded, and may be part of the reason why the amplitude of variability is smaller at optical wavelengths (see below). We have tested different source extraction radii (7, 5 and 3 arcsec), and the difference in the derived magnitudes is less than

the standard deviation in each filter of about 0.15 mag. The smaller extraction radius was accounted for by setting the *wotsource* parameter *apercorr* to *curveofgrowth*. However, we also note that in our optical spectrum of RXJ2317.8–4422 (Grupe et al. 2004) no host absorption features are detected, arguing against the dominance of host emission in the optical.

2.2 XMM-Newton

XMM-Newton (Jansen et al. 2001) visited RX J2317–4422 twice. The first observation was performed on 2014 October 29 (MJD 56960) for a total of 16.9 ks (Table 2). This observation was an initial observation to check on the state of the source and to obtain a low state spectrum. After this observation confirmed the low state we triggered a second, 104 ks, observation starting on 2014 November 16 22:48 UT (MJD 56978). This observation was performed simultaneously with *NuSTAR* (see below) and *Swift*.

The EPIC pn camera (Strüder et al. 2001) was operating in Full Frame mode with a thin UV-blocking filter. Only PATTERN 0-4 (single and double events) were accepted for further analysis. Due to high energy background flares, part of the observations had to be discarded leaving net exposure times of 14900 s and 89081 s, respectively. The EPIC MOS 1 and 2 cameras (Turner et al. 2001) were operated in Full-Window mode with the thin filters. The exposure times were 16472s and 102954s for MOS 1 and 16441s and 102988s for MOS2, respectively. For the event selection, only PATTERN 0-12 (single to quadruple events) were accepted. In all three instruments source counts were selected in a circle with a radius of 32". The background counts were selected from a nearby source-free region with a radius of 64". The spectral data were binned with 20 counts per bin. In order to increase the statistical significance of the spectral fits, the data of all three instruments were analyzed simultaneously with *XSPEC* version 12.9.1p (Arnaud 1996).

2.3 NuSTAR

RX J2317–4422 was observed with *NuSTAR* (Harrison et al. 2013) for 150 ks from 2014 November 16, 17:25 UT (Table 2). We reduced the *NuSTAR* data using the *NuSTAR* Data Analysis Software (NuSTARDAS) version 1.5.1 and CALDB version 20150904. We filtered for background flares, and found clean on-source exposure times of 83.6 ks and 83.4 ks for FPMA and FPMB (the two *NuSTAR* focal plane modules), respectively. This is roughly half the duration of the observation, due to *NuSTAR*'s low-Earth orbit. We extracted source photons from a 30" circular region, centered on the source coordinates, and background photons from a 100" circular region on the same chip. The background is non-uniform across the detectors in this observation, so we position the background region as close as possible to the source region (we choose not to use an annular region, as it would overlap with the gap between chips). We combined the spectra from FPMA and FPMB using the *addspec* FTOOL. The spectrum is background-dominated over the full band, and RX J2317.8–4422 is only marginally detected at a 2.3σ level. The 3σ upper limit is 0.0013 counts s^{-1} which corresponds

to a 3–79 keV flux of 9×10^{-17} W m^{-2} . per detector. Due to the low number of counts we did not perform a spectral analysis of these data.

3 RESULTS

3.1 X-ray and UV Variability

The upper panel of Figure 1 displays the long-term 0.2–2.0 keV light curve of RX J2317–4422 starting with the RASS observation in November 1990 (MJD 48208). RX J2317–4422 was only observed once again by ROSAT with the High Resolution Imager in May 1997 (MJD 50575). The observation appeared to be a factor of 2 fainter compared with the RASS observation (Grupe et al. 2001). However, this is within the normal variability range of an AGN. RX J2317–4422 was not observed again by another X-ray observatory until May 2005 (MJD 53516) when it was observed by *Swift* as an X-ray calibration target. All *Swift* observations since May 2005 are listed in Table 1. It was only observed twice again as a fill-in target in April 2006 (Grupe et al. 2010) until we started revisiting RX J2317–4422 with further guest investigator (GI) fill-in programs to study the long-term X-ray and UV variability of AGN in general. Absorption/reddening corrected fluxes in the 0.3–10 keV band (see Sect. 2.1) and in all 6 UVOT filters of all *Swift* observations are listed in Table 3. Note that the observed X-ray band corresponds to 0.34 - 11.34 keV in the rest-frame. Due to the low redshift and relatively low reddening in the direction of the AGN no k-correction was applied. While it still appeared to be in its "normal" state during the observation on 2013–July 23, it dropped significantly by a factor of at least 8 by 2014 April/May where only a 3σ upper limit was determined at a level of 2×10^{-16} W m^{-2} . Another *Swift* observation in 2014 September suggested a drop by factor of 12 when compared with the last detection in 2013 July. This drop by a factor of >10 motivated us to trigger pre-approved *XMM-Newton* and *NuSTAR* observations. The flux levels of the two *XMM-Newton* observations in the 0.2–2.0 keV band are displayed as open triangles in Figure 1. The 0.3–10 keV fluxes during the *XMM-Newton* observations were about 7×10^{-17} W m^{-2} and 2.5×10^{-17} W m^{-2} , respectively. During both observations, the count rate in the *Swift* XRT was too low to obtain a detection. During most low-state observations *Swift* was unable to detect the AGN and only 3σ upper limits were obtained. Nevertheless, we got *Swift* XRT detections several times including the most recent observation on 2018–May-27 and December-28 when it was found at a level of about 3×10^{-17} W m^{-2} in the 0.3–10 keV band.

The UVOT W2 light curve is displayed in the lower panel of Figure 1. The light curves of the UVOT U, W1, M2, and W2 filters are shown in Figure 2. Table 3 also lists the mean, median and standard deviation values of the fluxes in the 0.3–30 keV band as well as all 6 UVOT filters. Clearly the strongest variability can be seen in X-rays, while the variability in the UVOT filters is lower, but still significant. The standard deviation in magnitudes is about 0.15 mag in each filter. While the long-term as well as the *Swift* XRT and UVOT light curves suggest strong variability in RX J2317–4422, the short-term light curve obtained during the 100 ks

Table 1. *Swift* Observation log of RX J2317.8-4422

ObsID	Segment	T-start ¹	T-stop ¹	MJD	T _{XRT} ²	T _V ²	T _B ²	T _U ²	T _{UVW1} ²	T _{UVM2} ²	T _{UVW2} ²
56630	003	2005 May 26 08:08	2005 May 26 10:09	53516.380	1085	—	—	—	2445	—	—
35310	001	2006 Apr 18 00:18	2006 Apr 18 23:02	53843.444	7022	677	677	673	1343	1746	2745
	002	2006 Apr 20 05:18	2006 Apr 20 23:04	53845.340	3212	264	264	264	529	717	1075
91650	001	2013 May 03 13:41	2013 May 03 13:52	56415.574	185	61	61	61	122	38	244
	003	2013 Jul 23 05:21	2013 Jul 23 15:09	56496.413	3000	266	266	266	539	789	1079
91886	001	2014 Apr 20 05:26	2014 Apr 21 08:49	56767.802	1577	11	137	715	777	—	239
	002	2014 May 01 16:32	2014 May 01 19:58	56778.760	1086	72	104	104	207	200	415
35310	004	2014 Sep 24 00:55	2014 Sep 24 01:12	56924.044	944	80	80	80	159	238	319
	005	2014 Oct 20 10:12	2014 Oct 20 18:28	56950.594	562	82	82	82	204	249	327
	008	2014 Oct 29 22:48	2014 Oct 29 23:01	56959.955	687	59	59	59	119	147	238
80853	001	2014 Nov 16 17:44	2014 Nov 17 22:43	56978.260	1644	134	134	134	268	372	536
35310	009	2015 Apr 15 07:11	2015 Apr 15 12:11	57127.403	4845	125	125	125	3501	377	499
	010	2015 Aug 19 21:12	2015 Aug 19 21:34	57253.889	1271	105	105	105	209	332	420
	011	2015 Aug 24 21:13	2015 Aug 24 22:55	57258.917	1151	136	136	136	275	446	551
	012	2016 Apr 05 20:20	2016 Apr 05 23:55	57483.920	4500	127	127	127	3178	373	507
	013	2016 Dec 20 03:35	2016 Dec 20 08:34	57742.250	3544	40	117	117	153	122	259
	014	2016 Dec 24 03:21	2016 Dec 24 03:41	57746.147	455	96	96	96	192	255	385
93134	001	2017 Apr 19 13:02	2017 Apr 19 13:13	57862.547	649	52	52	52	103	160	207
	002	2017 Apr 25 06:11	2017 Apr 25 06:21	57868.260	569	43	43	43	85	149	172
35310	015	2018 May 27 06:38	2018 May 27 10:07	58265.351	4443	254	362	225	725	634	545
	016	2018 Dec 28 05:59	2018 Dec 28 09:36	58480.326	4765	391	391	391	783	1108	1036

¹Start and end times are given in UT²Observing time given in s**Table 2.** *XMM-Newton* and *NuSTAR* Observation log of RX J2317.8-4422

Mission	ObsID	T-start ¹	T-stop ¹	MJD	T _{obs} ²	T _{eff} ²
<i>XMM-Newton</i>	0740040101	2014-10-29 22:30	2014-10-30 02:41	56960.024	16911	14900
	0740040301	2014-11-16 22:48	2014-11-18 03:16	56978.585	90998	89081
<i>NuSTAR</i>	800001030002	2014-11-16 16:51	2014-11-18 10:41	56978.587	148161	

¹Start and end times are given in UT²Observing time (T_{obs} and the effective exposure time (t_{eff}) after correcting for times of high background flares are given in s. These are the times schedules and used for the EPIC pn.

XMM-Newton pn observation in November 2014 shows constant emission. The *XMM-Newton* pn light curve is shown in Figure 3 using a bin size of 2000s.

3.2 X-ray spectral analysis

3.2.1 High State 1990-2013

During the RASS observation in 1990 November the X-ray spectrum in the 0.1-2.4 keV band appeared to be very steep with an energy spectral index of $\alpha_x=2.5\pm 0.8$ (Grupe et al. 2001). This spectral slope is consistent with those obtained from the *Swift* observations in 2005 May and 2013 July with $\alpha_x=2.34\pm 0.35$ and $\alpha_x=2.34\pm 0.29$, respectively. All these observations indicate a very steep X-ray spectrum during the high state consistent with the AGN operating at a high L/L_{Edd} ratio (see also Grupe et al. 2010).

In order to obtain a higher significance of the fit, we combined all *Swift* data during the high state from 2005 to 2013 which resulted in a total exposure time of 14.4 ks. Due to the relatively low number of counts (about 180) we did not bin the spectrum and instead applied Cash statistics (Cash 1979) when fitting the data. All spectral fits were performed with the absorption parameter at $z=0$ fixed to

the Galactic value. All spectral fit results are summarized in the upper part of Table 4.

We started fitting the data with a simple absorbed power law model which resulted in a steep spectrum with a spectral index $\alpha_x=2.32\pm 0.13$. However this fit deviates strongly for energies above 1.5 keV as displayed in Figure 4 and the C-statistic value over the degrees of freedom is 225/171. Note that for display purposes we binned the spectrum shown here with 20 counts per bin. Next step was a fit with a combined blackbody plus power law spectrum. This model significantly improved the fit. We found a blackbody temperature of 99 eV and an underlying hard power law spectrum with $\alpha_x=0.88$. The C-stat value here is 169/169. The unfolded spectrum of this fit, again using for display purposes a binning of 20 counts per bin, is shown in Figure 5. Although this is a phenomenological model, it fits the spectrum quite well. What this model may suggest is the presence of an underlying starburst.

A deviation from a simple power law model is typically a sign of the presence of a partial covering absorber or X-ray reflection (Gallo 2006).¹ Next, we applied both a redshifted

¹ We checked the background level from this combined data set

Table 3. *Swift* X-ray and UVOT Fluxes¹ of RX J2317–4422

ObsID	Segment	MJD	F_X	V	B	U	UVW1	UVM2	UVW2
56630	003	53516.380	3.14±0.34	—	—	—	5.38±0.26	—	—
35310	001	53843.444	2.11±0.09	4.22±0.19	4.00±0.13	4.26±0.18	4.21±0.22	4.77±0.15	4.81±0.19
	002	53845.340	0.44±0.13	4.43±0.28	4.25±0.19	4.45±0.22	4.43±0.28	4.69±0.17	4.78±0.21
91650	001	56415.574	<1.13 ²	4.05±0.49	4.51±0.35	4.85±0.33	3.60±0.33	4.91±0.59	5.22±0.29
	003	56496.413	1.71±0.12	4.66±0.24	4.57±0.17	4.96±0.22	4.71±0.28	5.14±0.17	5.16±0.21
91886	001	56767.802	<0.21 ²	—	3.38±0.23	3.90±0.18	3.16±0.22	—	3.16±0.21
	002	56778.760	<0.20 ²	3.24±0.38	3.65±0.23	3.70±0.26	3.32±0.28	3.56±0.25	3.39±0.21
35310	004	56924.044	0.15±0.01	3.25±0.37	3.60±0.25	4.19±0.29	3.37±0.29	3.83±0.22	3.79±0.23
	005	56950.594	<0.37 ²	4.04±0.38	3.54±0.25	—	3.41±0.28	4.13±0.25	3.87±0.23
	008	56959.955	<0.51 ²	4.05±0.46	4.71±0.32	4.12±0.33	3.74±0.33	4.37±0.30	3.83±0.25
80853	001	56978.260	<0.25 ²	3.83±0.31	3.76±0.21	3.45±0.21	3.34±0.25	2.93±0.20	3.56±0.19
35310	009	57127.403	<0.10 ²	3.28±0.42	3.02±0.26	1.68±0.17	2.65±0.14	3.23±0.17	2.87±0.17
	010	57253.889	0.11±0.07	4.38±0.36	4.09±0.23	4.59±0.26	3.85±0.53	4.46±0.22	4.12±0.21
	011	57258.917	0.12±0.08	4.33±0.32	4.00±0.21	4.37±0.26	3.90±0.28	4.50±0.20	3.79±0.19
	012	57483.920	0.040±0.026	4.51±0.42	3.92±0.25	4.56±0.26	4.13±0.22	4.67±0.21	4.31±0.21
	013+014	57744.146	<0.12 ²	4.13±0.76	4.30±0.30	4.01±0.22	3.85±0.22	4.27±0.30	4.30±0.19
93134	001+002	57865.375	<0.38 ²	3.71 ±1.01	3.42±0.44	3.79±0.40	3.04±0.30	3.66±0.27	3.33±0.23
35310	015	58265.351	0.033±0.016	3.99±0.30	3.71±0.13	2.92±0.13	3.18±0.14	3.39±0.12	3.10±0.11
	016	58480.326	0.038±0.018	2.95±0.17	2.85±0.14	3.26±0.11	2.99±0.11	3.49±0.10	3.33±0.10
	mean		0.714	3.921	3.840	3.911	3.967	4.109	3.926
	median		0.120	4.045	3.760	4.065	3.505	4.200	3.830
	standard deviation σ		1.088	0.509	0.528	0.813	0.688	0.677	0.731

¹All fluxes are given in units of 10^{-15} W m⁻². The UVOT fluxes are corrected for reddening with $E_{B-V}=0.037$ given by [Schlegel et al. \(1998\)](#). The X-ray fluxes are in the 0.3–10 keV range and are corrected for Galactic absorption [Kalberla et al. \(2005\)](#).

² 3σ upper limit determined using the Bayesian method as described in [Kraft et al. \(1991\)](#).

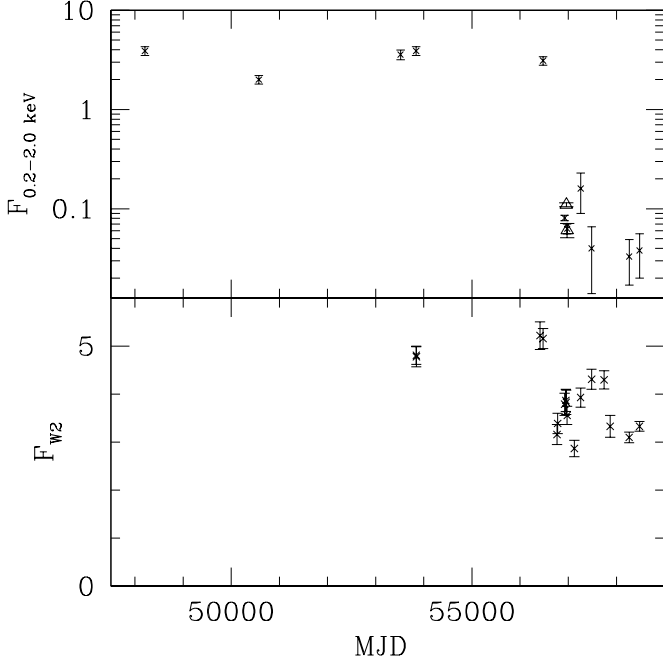


Figure 1. Long-term 0.2–2.0 keV light curve of RX J2317–4422 corrected for Galactic absorption (upper panel) The first observation was performed during the RASS in November 1990 (MJD = 48208) and the second observation by the ROSAT HRI in May 1997 ([Grupe et al. 2001](#)) at MJD=50515. The triangles mark the two *XMM-Newton* observations (MJD 56960 and 56978). All other observations were obtained by *Swift* (See Table 1). The lower panel displays the *Swift* UVOT W2 flux light curve. All fluxes are given in units of 10^{-15} W m².

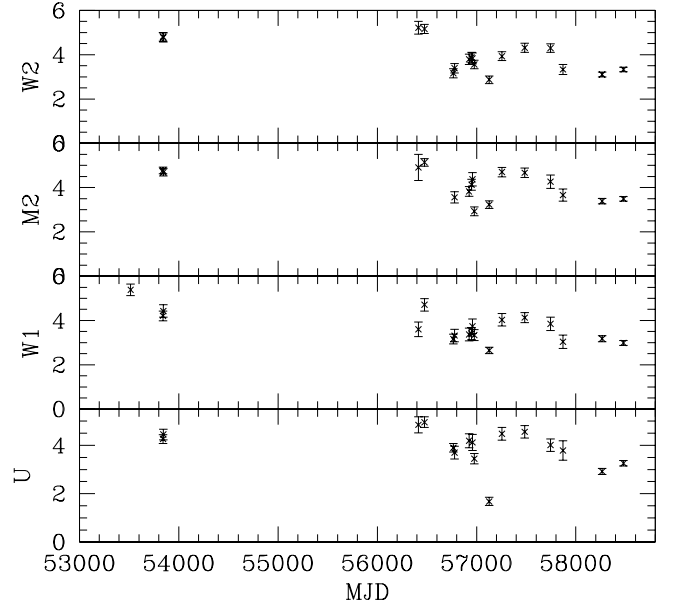


Figure 2. UVOT UV light curves of RX J2317–4422. All fluxes are given in units of 10^{-15} W m² and are listed in Table 3.

neutral partial covering absorber and an ionized partial cov-

and the contribution of background even at higher energies is negligible. The source counts account for 96.6% of the total number of counts extracted at the source position.

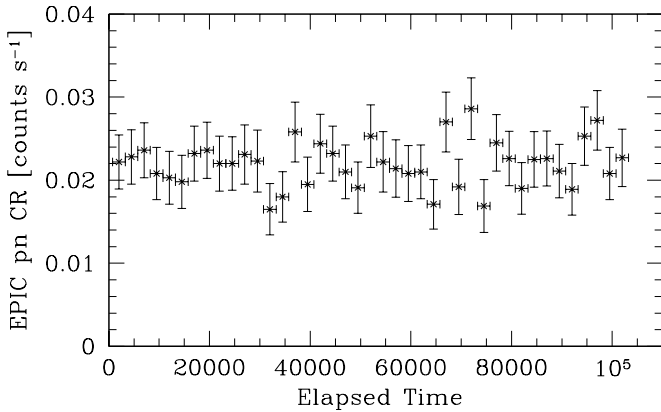


Figure 3. *XMM-Newton* EPIC pn 0.2-2.0 keV light curve during the 2014 November observation using a bin size of 2000s.

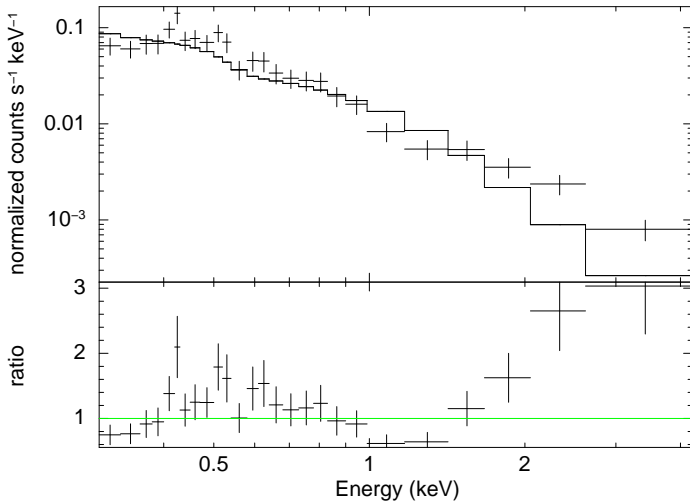


Figure 4. Combined spectrum of all high state data from *Swift* fitted with a single power law model. For display purposes we used the spectrum that was binned with 20 counts per bin.

ering absorber model. Both model fits resulted in similar C-stat values of 194/169 and 198/170, respectively. While the neutral pc models showed an absorption column density of $5.5 \times 10^{22} \text{ cm}^{-2}$, the absorption column density of an ionized partially-covering absorber was $1.3 \times 10^{23} \text{ cm}^{-2}$. The ionization parameter ξ was fixed to 10 (in units of $10^{-9} \frac{\text{Wm}^{-2}}{\text{m}^{-3}}$ or $\frac{\text{ergs}^{-1} \text{cm}^{-2}}{\text{cm}^{-3}}$). The underlying power law emission spectrum ($\alpha_x=2.82$) results in a flux in the 0.3-10 keV band of $3.5 \times 10^{-14} \text{ W m}^{-2}$.

Often reflection models also provide good solutions for spectra like this. Fitting with *reflionx* (Ross et al. 1999; Ross & Fabian 2005) and the blurred accretion disc model *kdblur* did result in a good fit with a C-stat value of 175/173. The partial covering absorber models and the reflection model produce similar fit results.

3.2.2 Low State after 2013

Due to the low X-ray flux state combined with the small effective area of the *Swift* XRT and the relatively short

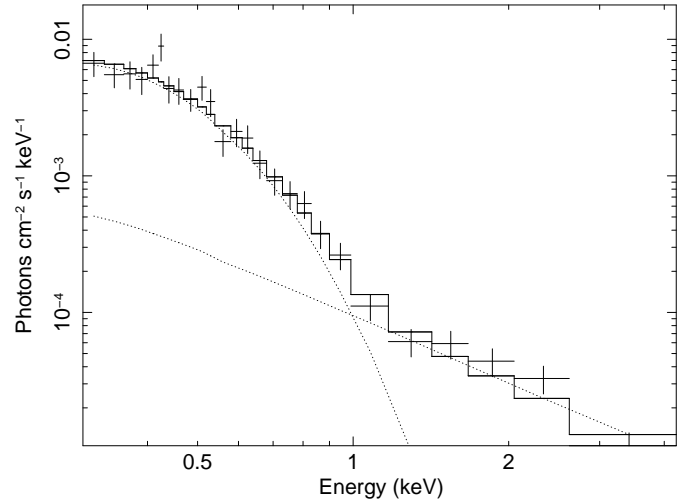


Figure 5. Unfolded combined spectrum of all high state data from *Swift* fitted with a blackbody plus single power law model. Again the binned spectrum shown here was only used for display purposes.

exposure times, none of the *Swift* observations during the low state allowed any kind of spectral analysis. Fluxes were determined by the count rate to flux conversion factor described in section 2.1. The spectral information of RX J2317–4422 can be obtained only from the *XMM-Newton* observations in 2014 October and November. For the spectral analysis the absorption column density was set to the Galactic value and the results of all spectral fits are listed in Table 4. The low X-ray flux of RX J2317–4422 in combination with the detector noise in the EPIC pn and MOS cameras made the data above 2 keV significantly background dominated. Therefore we restricted our analysis of the *XMM-Newton* low state data to the 0.2-2.0 keV energy range. As a consequence, complex spectral models like partial covering absorber or reflection models could not be applied.

For the *XMM-Newton* spectral data analysis we use a combined fit to all pn and MOS spectra where we organized the spectra into two data groups by the October and November 2014 spectra. We linked the fit parameters together except the normalizations. All results of the spectral fits to the *XMM-Newton* spectra are summarized in Table 4. Due to the background domination of the data above 2 keV no complex spectral analysis appears to be reliable. There is simply no handle on the data at higher energies which define parameters required to describe the partial covering absorber and reflection models. The only model, besides the standard single power law model, that we applied additionally to the data, was the black body plus power law model which results in a good fit. This fit is slightly better than that of the single power law model (T-test with T-value = 10.89 and P=0.001). What is interesting to note is that the blackbody component remains basically constant between the October and November observations, while the power law component drops by a factor of about 2.

The 2014 November *XMM-Newton* observation was performed simultaneously with *NuSTAR*. However, due to the low flux in the NuStar 5-79 keV band we could only obtain

Table 4. Spectral fits High State *Swift* data from 2005-2013 and the *XMM-Newton* EPIC pn and MOS low state spectra. The absorption parameter at $z=0$ was fixed to the Galactic value, $N_{\text{H}} = 1.07 \times 10^{20} \text{ cm}^{-2}$.

Model	α_x	kT ¹	$N_{\text{H, intr}}^2$	f_{pc}^2	ξ^3	$Norm_1^4$	$Norm_2^4$	cstat/dof or χ^2/ν
High State, <i>Swift</i> , Combined 2005-2013								
po	2.32±0.14	—	—	—	—	2.42×10 ⁻⁴	—	225/171
bb + po	0.87±0.34	99±7	—	—	—	2.48×10 ⁻⁵	1.14×10 ⁻⁴	169/169
zpcfabs * po	2.74±0.20	—	5.4 ^{+3.0} _{-1.7}	0.87 ^{+0.05} _{-0.09}	—	1.73×10 ⁻³	—	194/169
zxipcf * po	2.82 ^{+0.17} _{-0.16}	—	13.7 ^{+4.6} _{-4.8}	0.95	10	4.47×10 ⁻³	—	198/170
po + kdb * refl ⁵	1.37 ^{+0.16} _{-0.22}	—	—	—	220 ⁺³⁷⁷ ₋₁₀₂	1.09×10 ⁻⁵	1.44×10 ⁻⁷	175/173
Low State, <i>XMM-Newton</i> , 2014-October-30 and November-17								
po	2.65±0.16	—	—	—	—	9.69×10 ⁻⁶	—	202.7/173
bb + po	2.61 ^{+0.28} _{-0.18}	122 ⁺²⁶ ₋₂₁	—	—	—	1.44×10 ⁻⁷	7.94×10 ⁻⁶	190/172
						1.27×10 ⁻⁷	4.01×10 ⁻⁶	

¹kT given in units of eV

²The intrinsic absorption column density at the redshift of the AGN is given in units of 10^{22} cm^{-2} . Note if no uncertainty is given for the covering fraction f_{pc} then it was fixed to the given value.

³ ξ is the ionization parameter $\xi = \frac{L}{nr^2}$ given in units of $10^{-9} \frac{\text{Wm}^{-2}}{\text{m}^{-3}}$ or $\frac{\text{ergs s}^{-1} \text{cm}^{-2}}{\text{cm}^{-3}}$.

⁴the Normalizations $Norm_1$ and $Norm_2$ for the first and second model are given in units of 10^4 photons $\text{m}^{-2} \text{ s}^{-1} \text{ keV}^{-1}$ at 1 keV. For the low state data, the first row corresponds to the October 2014 *XMM-Newton* data and the second row to the November 2014 spectra.

⁵po + reflionx * kdblur model. The energy index α for the reflionx model was fixed to the energy index of the power law model. For the inner radius we assume a moderately rotating black hole with $r_{\text{in}} = 2r_g$. For the kdblur model the emissivity index was fixed to 5.0 and the inclination angle to 30° .

a 3σ upper limit at a flux level of $9 \times 10^{-17} \text{ W m}^{-2}$. Assuming the power law model found from the *XMM-Newton* data with a spectral slope $\alpha_x = 2.65$, this corresponds to a flux in the 5–79 keV band of $4 \times 10^{-18} \text{ W m}^{-2}$, which is consistent with the 3σ level derived from the *NuSTAR* data.

3.3 UVOT data

The UVOT W2 light curve is displayed in the lower panel of Figure 1 and it suggests significant variability in the UVOT filters. This variability may suggest color changes between different UVOT bands. We computed B-V, U-B, W2-U, and W2-W1 colors. The Spearman rank order correlation coefficients of the W2-U and W2-W1 colors are $\rho = 0.63$ and 0.56 with probabilities of a random distribution of $P = 0.015$ and 0.028 , respectively. A correlation analysis of the optical color shows that they are clearly uncorrelated.

Another question is, are the color changes in W2-U and W2-W1 colors correlated with the X-ray fluxes. Due to the small number of X-ray detections during the low state, this only allows a very limited analysis. Figure 6 displays the W2-U color vs. the 0.3–10 keV X-ray flux of RX J2317–4422. Although this plot suggests that the AGN has a blue UV spectrum when it is brighter in X-rays, due to the small number of data points any correlation analysis will be rather meaningless. Nevertheless we can apply a 2×2 contingency table. From these data we find that there is a 27% chance that the AGN is bright in X-rays and blue in the UV and a 73% chance that it is faint in X-rays and red in the UV. The chances of being faint in X-rays and blue in the UV and bright in X-rays and red in the UV are both 0.

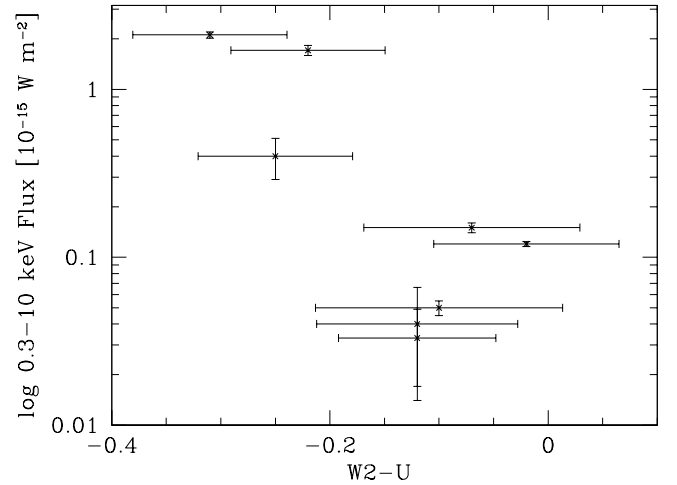


Figure 6. *Swift* UVOT W2-U color vs 0.3–10 keV X-ray flux of RX J2317–4422.

3.4 Spectral Energy Distribution

Figure 7 displays the spectral energy distributions during the high state seen in 2006 and the low state during the *XMM-Newton* and *NuSTAR* observation in November 2014. The high state is shown with the black stars and is based on the *Swift* observations. The low state data from November 2014 are using the *Swift* UVOT in the optical/UV and the *XMM-Newton* EPIC pn data for the X-ray range.

The high state X-ray spectrum seen in RX J2317–4422 is very soft suggesting a high L/L_{Edd} ratio. We went back to the original optical spectrum (Grupe et al. 2004) and recalculated the black hole mass of RX J2317–4422 using the FWHM($H\beta$) and the luminosity at 5100\AA as described in

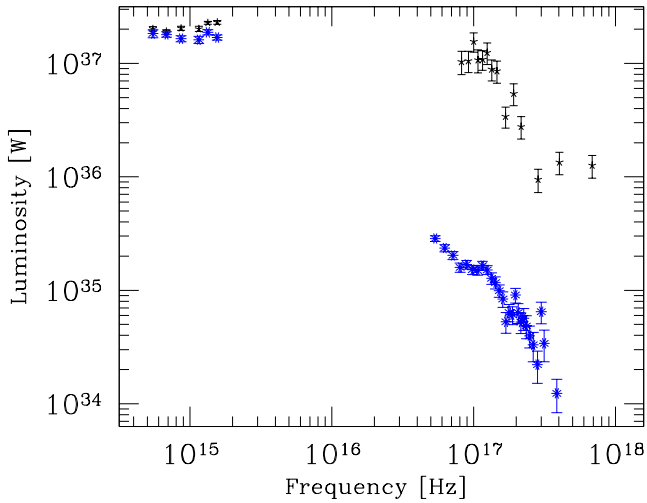


Figure 7. Spectral Energy distributions of RX J2317–4422 during the 2006 high state (black stars) and the low state in November 2014 (blue symbols).

Kaspi et al. (2000). We found that in Grupe et al. (2004) the black hole mass was underestimated by a factor of two. We found that the black hole mass is about $7.5 \times 10^6 M_{\odot}$.

The optical to X-ray spectral slope α_{ox}^2 changes from $\alpha_{\text{ox}} = 1.45$ during the high state in 2006 to $\alpha_{\text{ox}} = 2.07$ in the low state in November 2014. Given the luminosity density at 2500\AA of $\log(l_{2500}) = 22.24$ and following the $l_{2500} - \alpha_{\text{ox}}$ relation given in Grupe et al. (2010), the expected α_{ox} value is 1.36. The α_{ox} value during the high state is comparable with the expected value. The UV/Optical part of the SED as shown in Figure 7 appears to be rather flat and may suggest that the optical continuum has a significant host contribution, or is still dominated by the AGN which, however, suffers some extinction. The UV spectral slope $\alpha_{\text{UV}} = 2.0$ (Grupe et al. 2010) is rather red in particular for a NLS1. This may suggest intrinsic reddening and not a significant contamination by the host. As mentioned earlier, there are no obvious stellar absorption line features in the optical spectrum (Grupe et al. 2004) which also argues from reddening of the AGN emission rather than host galaxy contamination.

RX J2317–4422 is not detected in the Parkes-MIT-NRAO (PMN) radio survey at 4.85 GHz (Wright et al. 1994). Considering that the upper limit in the Southern survey is at 20 mJy ($2 \times 10^{-28} \text{ W m}^{-2} \text{ Hz}^{-1}$) and that the flux in the *Swift* UVOT B-band is of the order of $3.6 \times 10^{-15} \text{ W m}^{-2}$ or flux density of 0.5 mJy results in an upper limit of the radio loudness of $R < 40$ applying the definition by Kellermann et al. (1989).

4 DISCUSSION

4.1 On the nature of the X-ray low-state of RX J2317–4422

While almost all AGN are variable in X-rays, drops by factors ~ 100 or more are relatively rare. These strong changes, along with spectral complexity, provide us with important

insights in the physics of the innermost central region of AGN. Variability and spectral complexity is often strongest in the class of NLS1 galaxies (review by Gallo 2018), of which RX J2317–4422 is a member. The majority of (radio-quiet) AGN with dramatic flux changes has been explained by one of the following mechanisms:

- A change in the accretion rate, for instance through an accretion disc instability or a tidal disruption event.
- Changes in the effects of (relativistically blurred) reflection of coronal X-ray emission off the accretion disc.
- Changes in (neutral or ionized) absorption along our line of sight, partially or fully covering the continuum source.

We now comment on (variants of) each of these mechanisms in application to RX J2317–4422.

4.1.1 TDE-like accretion event.

Most events of stellar tidal disruptions (TDEs) by SMBHs have been observed in non-active galaxies, and their X-ray emission rapidly fades away on the timescale of months to years (review by Komossa 2017). Recently, several long-lasting, decade-long events have been identified (Lin et al. 2017), which share with RX J2317–4422 the spectral softness at high-state and evidence for near- or super-Eddington accretion. However, RX J2317–4422 has been in its bright state for decades, implausibly long for a TDE, and also shows a classical NLR, indicating long-lasting classical AGN activity.

4.1.2 Long-term changes in accretion rate.

On timescales of years or decades, changes in the accretion rate can lead to fading of the (X-ray and UV) continuum emission (e.g. Noda and Done 2018; Dexter and Begelman 2018; Lawrence 2018; Ross et al. 2018, and references therein). In recent years, several such AGN have been found that seem to be slowly switching off, i.e., decreasing their accretion rates on the timescale of decades. The best of these cases show a systematic fading of their broad emission lines, implying a corresponding true intrinsic decrease in the ionizing (EUV) continuum emission (e.g. Denney et al. 2014). RX J2317–4422 likely does not fall in this category, since its X-ray light-curve does not show a slow fading, but a rather abrupt drop from a (long-lasting) high-state into a (still ongoing) deep low-state.

4.1.3 Reflection models.

When we see a strong hardening of the X-ray spectrum towards higher energy, a possible explanation is reflection of X-ray photons on the accretion disc (Ross et al. 1999; Ross & Fabian 2005, e.g.). Although these models can be successfully applied to the *Swift* high-state data, due to the dominating background in the *XMM-Newton* and *NuSTAR* observations during the low state, no conclusions can be drawn from these data. A deep long-duration observation with *XMM-Newton*, as recently carried out for IRAS 13224–3809 (Parker et al. 2017) would be required to break model degeneracies, and constrain the reflection (and any other model) components.

² $\alpha_{\text{ox}} = -0.384 \times \log(f_{2\text{keV}}/f_{2500})$; Tananbaum et al. (1979)

4.1.4 Absorption along our line of sight with or without starburst component.

Changes in our line of sight (cold or ionized) absorption are known to have strong effects on the observed soft X-ray spectra, and can therefore cause high-amplitude X-ray variability. High-amplitude absorption variability has been identified in intermediate-type Seyfert galaxies and BAL quasars, for instance (e.g. Gallagher et al. 2004; Risaliti et al. 2005; Bianchi et al. 2009). In several systems, simultaneous UV and X-ray absorption has been detected (e.g. Mkn 1048: Parker et al. 2014; Ebrero et al. 2016). In the extreme case of WPVS007, an X-ray drop by a factor of several hundred was accompanied by extremely strong broad absorption line troughs in the UV (Grupe et al. 1995; Grupe et al. 2013; Leighly et al. 2015). Gallo (2006) distinguished between two types of NLS1 X-ray spectra, “simple systems” where we have a relatively direct view onto their accretion disc with little spectral complexity, and “complex systems”. Jin et al. (2017) suggested that those are systems where our line of sight passes through a clumpy accretion-disc wind. RX J2317–4422 might be in the second class of NLS1 galaxies. We have tested, whether *all* X-ray variability of RX J2317–4422 can be due to absorption. For the combined high-state *Swift* data we derived a column density of about $5 \times 10^{22} \text{ cm}^{-2}$. However, due to the low number of source counts above 2 keV during the low state, no parameters of the partial covering absorber could be determined reliably.

We have also tested, whether the soft X-ray emission during low-state can be due to an additional starburst component, which is barely detected during high-state, but becomes visible during low-state because of the faintness of the AGN emission. Such a model fits the low-state data well, and NLS1 galaxies are known to show strong starburst components (e.g. Sani et al. 2010). A (0.3–10) keV X-ray luminosity in the starburst component of $L = 2.5 \times 10^{34} \text{ W}$ is then required, which is relatively luminous, but still a factor of 10 below the most X-ray luminous starbursts (e.g. Komossa et al. 2003).

ACKNOWLEDGEMENTS

We thank our referee, Chris Done, for useful comments and suggestions that improved this paper. We would like to thank Neil Gehrels and Brad Cenko for approving our ToO requests and the *Swift* team for performing the ToO observations of RX J2317–4422. We also want to thank our Morehead State University students Mason Bush, Chelsea Pruett, Sonny Ernst, and Taylor Barber for looking through the *Swift* data to find AGN in low X-ray flux states. This research has made use of the NASA/IPAC Extragalactic Database (NED) which is operated by the Jet Propulsion Laboratory, Caltech, under contract with the National Aeronautics and Space Administration. Based on observations obtained with XMM-Newton, an ESA science mission with instruments and contributions directly funded by ESA Member States and NASA. This research has made use of the XRT Data Analysis Software (XRTDAS) developed under the responsibility of the ASI Science Data Center (ASDC), Italy. ACF acknowledges ERC Advanced Grant 340442.

REFERENCES

- Arnaud, K. A., 1996, ASP Conf. Ser. 101: Astronomical Data Analysis Software and Systems V, 101, 17
- Ballo, L.; Giustini, M.; Schartel, N.; Cappi, M.; Jimenez-Bailon, E.; Piconcelli, E.; Santos-Lleo, M.; Vignali, C., 2008, A&A, 483, 137
- Bianchi, S., et al., 2009, ApJ, 695, 781
- Brandt, W.N., Pounds, K.A., & Fink, H., 1995, MNRAS, 273, L47
- Breeveld, A.A., et al., 2010, MNRAS, 406, 1687
- Burrows, D., et al., 2005, Space Science Reviews, 120, 165
- Cardelli, J.A., Clayton, G.C., Mathis, J.S., 1989, ApJ, 345, 245
- Cash, W., 1979, ApJ, 228, 939
- Crawley, M.J., 2009, The R Book, John Wiley & Sons, Chichester, England
- Denney, K.D., et al., 2014, ApJ, 796, 134
- Dexter, J., Begelman, M., 2018, MNRAS, 483, L17
- Ebrero, J., Kriss, G.A., Kaastra, J.S., Ely, J.C., 2016, A&A, 586, 72
- Fabian, A.C., et al., 2012, MNRAS, 419, 116
- Gallagher, S.C., et al. 2004, ApJ, 603, 425
- Gallo, L.C., 2006, MNRAS, 368, 479
- Gallo, L.C., Grupe, D.; Schartel, N.; Komossa, S.; Miniutti, G.; Fabian, A. C.; Santos-Lleo, M., 2011, MNRAS, 412, 161
- Gallo, L.C., et al. 2013, MNRAS, 438, 1191
- Gallo, L.C., et al., 2015, MNRAS, 446, 633
- Gallo, L.C., Blue, D.M., Grupe, D., Komossa, S., & Wilkins, D.R., 2018, MNRAS, 478, 2557
- Gallo, L., 2018, Proceedings of Science, PoS (NLS1-2018) 034
- Gehrels, N., et al., 2004, ApJ, 611, 1005
- Grupe, D., 2004, AJ, 127, 1799
- Grupe, D., et al., 1995a, A&A, 299, L5
- Grupe, D., Beuermann, K., Mannheim, K., Thomas, H.-C., de Martino, D., & Fink, H.H., 1995, A&A, 300, L21
- Grupe, D., Beuermann, K., Thomas, H.-C., Mannheim, K., & Fink, H.H., 1998, A&A 330, 25
- Grupe, D., Beuermann, K., Mannheim, K., & Thomas, H.-C., 1999, A&A, 350, 805
- Grupe, D., Leighly, K.M., Thomas, H.-C., & Laurent-Muehleisen, S.A., 2000, A&A, 356, 11
- Grupe, D., Thomas, H.-C., & Beuermann, K., 2001, A&A, 367, 470
- Grupe, D., Wills, B.J., Leighly, K.M., & Meusinger, H., 2004, AJ, 127, 156
- Grupe, D., Komossa, S., Gallo, L.C., Fabian, A.C., Larsson, J., Pradhan, A.K., Xu, D., & Miniutti, G., 2008, ApJ, 681, 982
- Grupe, D., Leighly, K.M., & Komossa, S., 2008, AJ, 136, 2343
- Grupe, D., Komossa, S., Leighly, K.M., & Page, K.L., 2010, ApJS, 187, 64
- Grupe, D., Komossa, S., Gallo, L.C., Longinotti, A.L., Fabian, A.C., Pradhan, A.K., Gruberbauer, M, & Xu, D., 2012, ApJS, 199, 28
- Grupe, D., Komossa, S., Scharwächter, J., Dietrich, M., Leighly, K.M., Lucy, A., & Barlow, B.N., 2013, AJ, 146, 78
- Grupe, D., Komossa, S., & Saxton, R., 2015, ApJ, 803, L28
- Guainazzi, M., et al., MNRAS, 301, L1
- Harrison, F.A., et al., 2013, ApJ, 770, 103
- Hill, J.E., et al., 2004, SPIE, 5165, 217
- Jansen, F., et al., 2001, A&A, 365, L1
- Jin C., Done C., Ward M., Gardner E., 2017, MNRAS, 471, 706
- Kalberla, P.M.W., et al., 2005, A&A, 440, 775
- Kaspi, S., Smith, P.S., Netzer, H., Moaz, D., Jannuzi, B.T., & Giveon, U., 2000, ApJ, 533, 631
- Kellermann, K.I., Sramek, R., Schmidt, M., Shaffer, D.B., & Green, R., 1989, AJ, 98, 1195
- Kraft, R.P., Burrows, D.N., & Nousek, J.A., 1991, ApJ, 374, 344
- Kollatschny, W.; Schartel, N.; Zetzl, M.; Santos-Lleo, M.;

- Rodriguez-Pascual, P. M.; Ballo, L., 2015, *A&A*, 577, 1
- Kollatschny, W.; Schartel, N.; Zetzl, M.; Santos-Lleo, M.; Rodriguez-Pascual, P. M.; Ballo, L.; Talavera, A., 2016, *A&A*, 585, 18
- Komossa, S.; Bade, N., 1999, *A&A*, 343, 775
- Komossa, S.; Fink, H., 1997, *A&A*, 327, 483
- Komossa, S., et al., 2003, *ApJ*, 582, L15
- Komossa, S.; Grupe, D.; Saxton, R.; Gallo, L., 2014, *PoS(SWIFT 10)*143
- Komossa, S., 2017, *AN*, 338, 256
- Komossa, S.; Grupe, D.; Schartel, N.; Gallo, L.; Gomez, J.L.; et al., 2017, *IAUS*, 324, 168
- Lawrence, A., 2018, *NatAs*, 2, 102
- Laor, A., 1991, *ApJ*, 376, 90
- Leighly, K.M., Hamann, F., Casebeer, D.A., & Grupe, D., 2009, *ApJ*, 701, 176
- Leighly, K.M., Cooper, E., Grupe, D., Terndrup, D.M., & Komossa, S., 2015, *ApJ*, 809, L13
- Lin, D., et al., 2017, *NatAs*, 1, 33
- Magdziarz, A., & Zdziarski, A.A., 1995, *MNRAS*, 273, 837
- Mason, K.O., et al., 2001, *A&A*, 365, L36
- Mizumoto, M., et al., 2014, *PASJ*, 66, 122
- Noda, H., Done, C., 2018, *MNRAS*, 480, 3898
- Park, T., Kashyap, V.L., Siemiginowska, A., van Dyk, D.A., Zezas, A., Heinke, C., & Wargelin, B.J., 2006, *ApJ*, 652, 610
- Parker, M.L., Schartel, N., Komossa, S., Grupe, D., Santos-Lleo, M., Fabian, A.C., & Mathur, S., 2014, *MNRAS*, 445, 1039
- Parker, M.L., et al., 2016, *MNRAS*, 461, 1927
- Parker, M., et al., 2017, *Nature*, 543, 83
- Poole, T.S., et al., 2008, *MNRAS*, 383, 627
- Poutanen, J., & Svensson, R., 1996, *ApJ*, 470, 249
- Risaliti, G., et al., 2005, *ApJ*, 623, L93
- Roming, P.W.A., et al., 2005, *Space Science Reviews*, 120, 95
- Roming, P.W.A., et al., 2009, *ApJ*, 690, 163
- Ross, R.R. & Fabian, A.C., 2005, *MNRAS*, 358, 211
- Ross, R., Fabian, A.C., & Young, A.J., 1999, *MNRAS*, 306, 461
- Ross, N., et al., 2018, *arXiv1805.06921*
- Sani, E., et al., 2010, *MNRAS*, 403, 1246
- Saxton, R.D., Read, A.M., Esquej, P., Freyberg, M.J., Altieri, B., Bermejo, D., 2008, *A&A*, 480, 611
- Schartel, N.; Rodriguez-Pascual, P. M.; Santos-Lleo, M.; Ballo, L.; Clavel, J.; Guainazzi, M.; Jimenez-Bailon, E.; Piconcelli, E., 2007, *A&A*, 474, 431
- Schartel, N., Rodriguez-Pascual, P. M., Santos-Lleo, M., Jimenez-Bailon, E., Ballo, L.; Piconcelli, E. 2010, *A&A*, 512, 75
- Schlegel, D. J., Finkbeiner, D. P., & Davis, M. 1998, *ApJ*, 500, 525
- Schwope, A., et al., 2000, *AN*, 321, 1
- Strüder, L., et al., 2001, *A&A*, 365, L18
- Tananbaum, H., et al., 1979, *ApJ*, 234, L9
- Turner, M.J., et al., 2001, *A&A*, 365, L27
- Turner, T.J.; Reeves, J.N.; Braitto, V.; Costa, M., 2018, *MNRAS*, 476, 1258
- Voges, W., Aschenbach, B., Boller, T., et al., 1999, *A&A*, 349, 389
- Wilkins, D.R., Gallo, L.C., Grupe, D., Bonson, K., Komossa, S., & Fabian, A.C., 2015, *MNRAS*, 454, 4440
- Wright, A.E., Griffith, M.R., Burke, B.F., & Ekers, R.d, 1994, *ApJS*, 91, 111
- Wright, E.L., 2006, *PASP*, 118, 1711
- Yamasaki, H.; Mizumoto, M.; Ebisawa, K.; Sameshima, H., 2016, *PASJ*, 68, 80
- Zetzl, M., Kollatschny, W., Ochmann, M., Grupe, D., Haas, M., Ramolla, M., Chelouche, D., Kaspi, S., & Schartel, N., 2018, *A&A*, 618, 83
- Zhang, F.; Yu, Q.; Lu, Y., 2017, *ApJ*, 845, 88

This paper has been typeset from a $\text{\TeX}/\text{\LaTeX}$ file prepared by the author.